



# On the Applicability of Iron-Based Coatings Against Abrasion and Cavitation Erosion Wear

Tommi Varis<sup>1</sup> · Juha Lagerbom<sup>2</sup> · Tomi Suhonen<sup>3</sup> · Sakari Terho<sup>4</sup> · Jussi Laurila<sup>1</sup> · Petri Vuoristo<sup>1</sup>

Submitted: 2 September 2022 / in revised form: 21 November 2022 / Accepted: 5 December 2022  
© The Author(s) 2022

**Abstract** Iron-based coatings are often considered as replacement of hard chromium and WC-Co, as they pose lower health and environmental impact. In many cases, the combination of mechanical and chemical properties of iron-based alloys may be satisfactory and their relatively low cost makes these coatings an interesting candidate for many applications. This study is inspired by opportunities to harden the iron-base materials by strain hardening, solid solution strengthening, and precipitation hardening. Already commercially available Fe-based coating materials with precipitates of mixed carbides and borides in the metastable austenitic matrix achieve a high hardness. In this study, the cavitation erosion and abrasion resistance of

various Fe-based coatings produced by HVAF and HVOF processes were investigated. Four experimental precipitates containing materials were prepared, and the sprayed coatings were tested for abrasive wear and cavitation erosion. In addition to precipitates, the contributions of martensite and retained austenite phases were investigated by influencing the microstructure through heat treatments, as the ability of these phases to influence ductility and toughness can be crucial to achieve the desired material properties. The properties of experimental and two commercial Fe-based alloys are compared with WC-Co and Cr<sub>3</sub>C<sub>2</sub>-NiCr coatings by property mapping.

**Keywords** abrasion · cavitation erosion · chrome replacement · HVAF · HVOF · iron alloys · wear resistant coatings

This article is an invited paper selected from presentations at the 2022 International Thermal Spray Conference, held May 4–6, 2022, in Vienna, Austria, and has been expanded from the original presentation. The issue was organized by André McDonald, University of Alberta (Lead Editor); Yuk-Chiu Lau, General Electric Power; Fardad Azarmi, North Dakota State University; Filofteia-Laura Toma, Fraunhofer Institute for Material and Beam Technology; Heli Koivuluoto, Tampere University; Jan Cizek, Institute of Plasma Physics, Czech Academy of Sciences; Emine Bakan, Forschungszentrum Jülich GmbH; Šárka Houdková, University of West Bohemia; and Hua Li, Ningbo Institute of Materials Technology and Engineering, CAS.

✉ Tommi Varis  
tommi.varis@tuni.fi

<sup>1</sup> Faculty of Engineering and Natural Sciences, Tampere University, Tampere, Finland

<sup>2</sup> VTT Technical Research Centre of Finland Ltd, Tampere, Finland

<sup>3</sup> VTT Technical Research Centre of Finland Ltd, Espoo, Finland

<sup>4</sup> Luvata, Pori, Finland

## Introduction

Due to material cost, health and environmental impact issues, alternatives are constantly being sought, especially for WC-Co/CoCr. Iron-based coatings are often considered as a good substitute because in many cases the combination of mechanical and chemical properties of iron-based alloys can be satisfactory and their relatively low cost makes these coatings an interesting alternative for many applications such as cylinder bores (Ref 1, 2), fluidized bed boilers (Ref 3-5), and for sliding, abrasion, and erosion wear applications in general (Ref 6-10). When comparing the performance of thermally sprayed wear-resistant coatings against erosion or abrasion, WC-Co/CoCr or Cr<sub>3</sub>C<sub>2</sub>-NiCr coatings are usually chosen as their performance may be difficult to achieve with alternative materials. Especially, abrasion wear resistance of WC-Co/CoCr has found to be

superior compared to Fe-based coatings (Ref 7). This is understandable, as abrasive wear is mainly characterised by micro-cutting, where the hard particle must penetrate the material and remove the material from the surface in the form of a chip. Thus, abrasive wear rate is reported to be controlled by such factors as hardness, carbide size, mean free path of carbides (Ref 11-13). However, in applications such as sliding and cavitation erosion wear, Fe-based materials appear to offer promising wear resistance. Bolelli et al. (Ref 6) showed that sliding wear performance of iron-based alloy (Fe-Cr-Ni-Cr-Fe-Si-B-C) was better compared to Ni-based (Ni-Cr-Fe-Si-B-C). Mahade et al. (Ref 9, 10) studied the adhesive wear of iron-based HVOF and HVOF coatings and showed that very low coefficient of friction (0.2) can be achieved with iron alloys, especially with HVOF sprayed Fe-CrNi-BCSi. With respect to cavitation erosion resistance, the properties of Fe-based thermally sprayed coatings have shown in some cases even better properties than thermally sprayed WC-CoCr coatings (Ref 14). Good cavitation erosion resistance iron-based coatings from atomised powders can be explained by a different wear mechanism compared to abrasive wear. Cavitation erosion wear can be considered as a cyclic fatigue loading, and the erosion rate is determined by the growth rate of the fatigue crack and the detachment of the resulting fractured areas. Fatigue cracks grow preferably along the weak lamellae boundaries. The hardness of the coating and the size of the carbides are less important compared to abrasion-induced erosion (Ref 15-17). Milanti et al. (Ref 14) showed that Mo increases the resistance to cavitation erosion, and they claimed that this is due to improved lamellar cohesion. Bolelli et al. (Ref 18) stated that good cavitation resistance may be a consequence of the material's ability to strain harden. Although in the case of solid steels, it has been shown that martensitic transformation in steels can be exploited to improve their resistance to cavitation erosion (Ref 16-18), publications on the cavitation resistance of thermal sprayed iron-based coatings have mostly suggested that good cavitation erosion resistance is mainly due to the high hardness of the coating caused by carbide and boride precipitates in the coating and the positive effect of strain hardening has not been extensively discussed (Ref 8, 11, 19).

A relatively wide range of thermally sprayable iron-based powders, which form chromium carbide hard phases, are available from commercial suppliers with a compositional basis of Fe-Cr-Ni-C. The concentration of Cr and C in such a material induces the formation of  $\text{Cr}_3\text{C}_2$ ,  $\text{Cr}_7\text{C}_3$ ,  $(\text{Cr,Fe})_{23}\text{C}_6$ , and  $(\text{Cr,Fe})_2\text{B}$  precipitates, which contributes to hardness, while Ni stabilizes austenite phase in the matrix (Ref 14). High concentrations of chromium and nickel also improve corrosion resistance (Ref 19). Si and B are also often added, which increase hardness by forming

precipitates (Ref 20), but also increase the tendency to amorphousness, which may increase the brittleness of the material (Ref 14, 21, 22). Amorphous coatings are also being developed for their specific corrosion resistance properties and hardness. On the other hand, the heat treatment of an amorphous alloy, which is basically a supersaturated mixture, produces nano-sized precipitates that effectively strengthen coatings. (Ref 20-26). For example, Huang et al. (Ref 26) showed that erosion-corrosion wear resistance of amorphous Fe-alloy (Fe<sub>48</sub>Cr<sub>15</sub>-Mo<sub>14</sub>C<sub>15</sub>B<sub>6</sub>Y<sub>2</sub>, at.%) can be improved by crystallisation/precipitation heat treatment and Yuping et al. (Ref 20) showed very good cavitation erosion resistance for amorphous/nanocrystalline Fe-Cr-Si-Mn-B alloy compared to martensitic stainless steel.

Vanadium carbide (VC) is an interesting hard phase, as its hardness is comparable to WC and clearly harder than chromium-based carbides. Thus, it is widely used in tool steels to produce carbide precipitates, which effectively increase hardness. In addition, due to the high formation temperature of VC, carbides are already formed in the molten state, and in high vanadium content alloy they can grow relatively large during the atomization process (Ref 27). For example, Wielage et al. (Ref 28) investigated the two and three body abrasion resistance of coatings sprayed with vanadium- and carbon-rich powders (Fe-26.5Cr-21V-9Co-4B-1.8C) and (Fe-16V-13Cr-4C-W-Mo). They showed that powders with high vanadium carbide content can be prepared by atomization and the sprayed coatings had excellent two-body and three-body abrasion wear resistance. However, the corrosion resistance was not sufficient due to microcracks in the coating.

The microstructure of a thermally sprayed coating is formed by very rapid cooling, so it will not form an equilibrium microstructure. In addition, the cohesion of lamellar boundaries produced by the splats and their oxidation have a detrimental effect on the extractable properties of the coating. This makes it very difficult to control the microstructure of a thermally sprayed coating in the same way as the microstructure of a precisely heat-treated material produced by other methods. However, there is a need for a better understanding of the potential of iron-based coatings. This study addresses the wear and cavitation erosion resistance of different types of iron-based high velocity oxy-fuel (HVOF) and high velocity air-fuel (HVOF) coatings. Both commercial and experimental atomized iron-based alloys were selected for the study to produce coatings with different types of microstructures. Agglomerated and sintered WC-CoCr and  $\text{Cr}_3\text{C}_2$ -NiCr coatings were used as reference materials. Wear resistance and cavitation erosion wear resistance were tested using the rubber wheel and indirect cavitation erosion test methods. In addition, the influence of HVOF and HVOF processes

and different HVOF parameters or gun configurations on the microstructure and wear resistance of the coating were investigated. The HVOF and HVAF processes are known to produce different thermal histories for spray particles, since combustion of oxygen-propane in the HVOF process produces a much higher flame temperature than combustion of air-propane in the HVAF process (Ref 17, 29).

## Experimental

The study used two different commercial atomized Fe powders and four experimental Fe powders, which were compared with commercial WOKA 3654 WC-CoCr powder (WC-Com) from Oerlikon Metco and Amperit 588 Cr<sub>3</sub>C<sub>2</sub>-NiCr powder (CrC-Com) from Höganäs. The commercial Fe-based powders were Durmat 512 from Durum Verschleißschutz and Diamalloy 1010 from Oerlikon Metco. These were denoted by the code Fe-Com 1-2. Four different experimental iron alloy powders were prepared by atomization and labelled Fe-Exp 1-4. Experimental powders were manufactured using Hermiga 75/5VI high-pressure gas atomization unit from Phoenix Scientific Industries Ltd, East Sussex, UK. Atomisation was made in Ar-gas. The atomizer included induction melting furnace and bottom pour tapping crucible. In atomization, 5 kg batch of each experimental alloy was inductively melted. The melt was overheated to 200 °C above the melting temperature of alloys to ensure melt flow. The melt is then fed at 0.25 bar overpressure into a melt nozzle with diameter of 2 mm. The melt flow was atomized to droplets by laminar atomization nozzle with 60 bar argon gas. Gas-to-melt ratio was 3.5. After atomization, the powders were sieved to a suitable fraction. The experimental powder with the composition of Fe-5Cr-9V-8W-2B-1Ti-2.4C was labelled Fe-Exp1, and powder with the composition of Fe-12V-5Cr-1.5Mo-0.6Mn-1Si-2.4C was labelled Fe-Exp5. The part of the experimental powder batch with the composition Fe-11.5Cr-1V-0.7Mo-0.25Si-0.35Mn-1.55C was remained to as-atomized state and labelled Fe-Exp2 and part of the batch then subjected to a heat treatment for 2 h in Ar atmosphere at 550 °C, with the purpose of harden the possible retained austenite in the powder. This experimental heat-treated powder was labelled as Fe-Exp 3. The crystalline structure of coatings was determined by x-ray diffractometry (XRD: Empyrean, PANalytical, Netherlands) using Cu-K $\alpha$  radiation (1.5406 Å, 40 kV and 45 mA). Phase identification was done with HighScore PLUS software (PANalytical, Netherlands). The composition of powders and the nominal particle size distribution of commercial powders or measured particle size distribution of experimental powders are shown in Table 1. Malvern Master sizer 3000 (Malvern Panalytical, UK) laser

diffraction analyser was used for measuring the particle size of experimental powders. The cross section of powders was studied using Zeiss ULTRA plus UHR FESEM microscope (Carl Zeiss AG, Oberkochen, Germany).

Coatings were sprayed using high kinetic processes: HVOF gun was Diamond Jet Hybrid 2700 (propane) from Oerlikon Metco AG (Wohlen, Switzerland) and HVAF gun was M3 from Uniquecoat Technologies LLC (Oilville, USA). Details of the spraying parameters are given in Table 2. Coatings were applied on (150 × 50 × 5) mm steel substrate using a robot with 0.9 m/s traverse speed and a step width of 3.5 mm. The substrate temperature was monitored during spraying with a Fluke Ti300 (Everett, WA, USA) thermal imager, which allowed the temperature of the sample to be kept approximately at 200 °C.

For structural studies, cross-sectional specimens of the coatings were prepared by cutting with a precision cutter, casting in resin, and grinding and polishing. Microstructural analysis of the cross-sectional samples was performed using a JEOL JSM-IT500 (Tokyo, Japan) scanning electron microscope (SEM) in backscattered electron (BSE) mode using a 15 kV acceleration voltage and a working distance of approximately 10 mm. Coating Vickers hardness was measured using an EMCOTEST hardness tester by Struers GmbH, Kuchl Germany. Hardness was measured on the polished cross sections at a load of 300 g. Ten indentations were performed on each coating.

Samples were tested according to ASTM G32-16 “standard test method for cavitation erosion using vibratory apparatus”. In the test, specimens of size (25 × 25 × 5) mm, grinded with 4000 grit SiC paper, were placed in distilled water and a high-frequency vibrating tip was placed at a distance of 500 μm from the specimen. An ultrasonic transducer VCX-750 from Sonics and Materials, USA, was used for the tests. The vibration caused bubbles to form and collapse in the liquid, and the collapsing bubbles cause damage and erosion (loss of material) of the sample. The vibrating tip was Ti-6Al-4V and tip diameter was 15.9 mm. The frequency in the test was 20 kHz and amplitude 50 μm. Water temperature was kept at 25 °C. The samples were weighed with high accuracy scale after 15, 30, 60, 120, 240, and 360 min. Prior to weighing the samples were cleaned in an ultrasonic bath with ethanol and dried.

Abrasion wear behaviour of the coatings was evaluated using a modified version of the ASTM G65 dry sand-rubber-wheel abrasion wear test, where five samples were tested simultaneously. Blocky-shaped dry quartz sand (SiO<sub>2</sub>) with a grain size ranging from 0.1 to 0.6 mm was used as the abrasive. The flow rate of the abrasive was 25 g/min. Sample surfaces were ground using grit 600 SiC paper before testing. During the test, the samples were pressed with a normal load of 23 N against a rotating rubber wheel with a surface speed of 1.64 m/s. The 60 min

**Table 1** Powders used in the study

Code	Composition	Manufacturer, Tradename	Powder type	Particle size distribution, $\mu\text{m}^*$
WC-Com HVOF	WC-10Co4Cr	Oerlikon Metco, WOKA 3654	Agglomerated & sintered	15-45
WC-Com HVOF		Oerlikon Metco, WOKA 3652		10-30
Cr-C-Com HVOF	Cr <sub>3</sub> C <sub>2</sub> -20(Ni20Cr)	Höganäs, Amperit 529.074	Agglomerated & sintered	15-45
Cr-C-Com HVOF		Höganäs, Amperit 588.059		10-30
Fe-Com1 HVOF	Fe-31Cr-12Ni-3.6B-0.6C	Durum, Durmat 512.007	Atomized	15-45
Fe-Com1 HVOF		Durum, Durmat 512.021		10-30
Fe-Com2 HVOF	Fe-28Cr-4.5Mo-16Ni-1.5Si-1.75C	Oerlikon Metco, Diamalloy 1010	Atomized	15-45
Fe-Com2 HVOF		Oerlikon Metco, Diamalloy 1010		15-45
Fe-Exp1 HVOF	Fe-5Cr-9V-8W-2B-1Ti-2.4C	VTT technical research centre of Finland, Experimental	Atomized	18-53
Fe-Exp1 HVOF				13-36
Fe-Exp2 HVOF	Fe-11.5Cr-1V-0.7Mo-0.25Si-0.35Mn-1.55C	VTT technical research centre of Finland, Experimental	Atomized	19-52
Fe-Exp2 HVOF				15-38
Fe-Exp3 HVOF	Fe-11.5Cr-1V-0.7Mo-0.25Si-0.35Mn-1.55C	VTT technical research centre of Finland, Experimental	Atomized, heat treated	19-52
Fe-Exp3 HVOF				15-38
Fe-Exp4 HVOF	Fe-12V-5Cr-1.5Mo-0.6Mn-1Si-2.4C	VTT technical research centre of Finland, Experimental	Atomized	17-50
Fe-Exp4 HVOF				17-50

\*Particle size distribution is the nominal size distribution for commercial powders and the D10-D90% value measured by laser diffraction for experimental powders

**Table 2** Spray parameters and sample codes

Code	Nozzle and Combustion Chamber	Propane	Oxygen	Air	Nitrogen	Spraying distance, mm	Powder feed rate	Thickness/pass, $\mu\text{m}$
WC-Com HVOF	2702	70 $\text{lm}^{-1}$	238 $\text{lm}^{-1}$	375 $\text{lm}^{-1}$	20 $\text{lm}^{-1}$	250	50 $\text{gm}^{-1}$	12.4
WC-Com HVAF1	4L2LargeCC	106 and 105 psi	...	108 psi	60 $\text{lm}^{-1}$	300	100 $\text{gm}^{-1}$	14.0
CrC-Com HVOF	2702	70 $\text{lm}^{-1}$	238 $\text{lm}^{-1}$	375 $\text{lm}^{-1}$	20 $\text{lm}^{-1}$	250	45 $\text{gm}^{-1}$	9.0
CrC-Com HVAF1	4L2LargeCC	106 and 105 psi	...	108 psi	60 $\text{lm}^{-1}$	300	100 $\text{gm}^{-1}$	15.0
Fe-Com1 HVOF	2702	70 $\text{lm}^{-1}$	238 $\text{lm}^{-1}$	375 $\text{lm}^{-1}$	20 $\text{lm}^{-1}$	250	40 $\text{gm}^{-1}$	18.4
Fe-Com1 HVAF1	4L2SmallCC	103 and 102 psi	...	107 psi	60 $\text{lm}^{-1}$	300	40 $\text{gm}^{-1}$	16.0
Fe-Com1 HVAF3	5L4SmallCC	115 and 110 psi	HIE 29	118 psi	60 $\text{lm}^{-1}$	300	40 $\text{gm}^{-1}$	16.0
Fe-Com2 HVOF	2702	70 $\text{lm}^{-1}$	238 $\text{lm}^{-1}$	375 $\text{lm}^{-1}$	20 $\text{lm}^{-1}$	250	40 $\text{gm}^{-1}$	14.0
Fe-Com2 HVAF1	4L2SmallCC	103 and 102 psi	...	107 psi	60 $\text{lm}^{-1}$	300	40 $\text{gm}^{-1}$	17.7
Fe-Com2 HVAF3	5L4SmallCC	115 and 110 psi	...	118 psi	60 $\text{lm}^{-1}$	300	40 $\text{gm}^{-1}$	7.5
Fe-Exp1 HVOF	2702	106 and 70 $\text{lm}^{-1}$	238 $\text{lm}^{-1}$	375 $\text{lm}^{-1}$	20 $\text{lm}^{-1}$	250	40 $\text{gm}^{-1}$	8.6
Fe-Exp1 HVAF1	4L2SmallCC	105 psi	...	118 psi	60 $\text{lm}^{-1}$	300	40 $\text{gm}^{-1}$	17.5
Fe-Exp1 HVAF2	4L4SmallCC	108 and 100 psi	...	114 psi	60 $\text{lm}^{-1}$	300	50 $\text{gm}^{-1}$	23.2
Fe-Exp1 HVAF3	5L4SmallCC	115 and 110 psi	...	121 psi	60 $\text{lm}^{-1}$	300	40 $\text{gm}^{-1}$	15.0
Fe-Exp2 HVOF	2702	70 $\text{lm}^{-1}$	238 $\text{lm}^{-1}$	375 $\text{lm}^{-1}$	20 $\text{lm}^{-1}$	250	40 $\text{gm}^{-1}$	14.4
Fe-Exp2 HVAF1	4L2SmallCC	103 and 102 psi	...	107 psi	60 $\text{lm}^{-1}$	300	40 $\text{gm}^{-1}$	16.5
Fe-Exp3 HVOF	2702	70 $\text{lm}^{-1}$	238 $\text{lm}^{-1}$	375 $\text{lm}^{-1}$	20 $\text{lm}^{-1}$	250	40 $\text{gm}^{-1}$	10.8
Fe-Exp3 HVAF1	4L2SmallCC	104 and 105 psi	...	108 psi	60 $\text{lm}^{-1}$	300	40 $\text{gm}^{-1}$	16.5
Fe-Exp4 HVOF	2702	70 $\text{lm}^{-1}$	238 $\text{lm}^{-1}$	375 $\text{lm}^{-1}$	20 $\text{lm}^{-1}$	250	40 $\text{gm}^{-1}$	14.0
Fe-Exp4 HVAF1	4L2SmallCC	106 and 105	...	108 psi	60 $\text{lm}^{-1}$	300	40 $\text{gm}^{-1}$	12.5
Fe-Exp4 HVAF2	4L4Small CC	110 and 100 psi	...	114 psi	60 $\text{lm}^{-1}$	300	40 $\text{gm}^{-1}$	6.7

test time used gives a wear length of 5904 m. The samples were weighed every 12 min using an analytical scale with 0.001 g accuracy.

## Results and Discussions

### Microstructural Features

The XRD analysis of experimental powders, in Fig. 1, reveals that Fe-Exp1 and Fe-Exp4 powders consist VC in the martensitic matrix. In Fe-Exp1 also some minor amount of  $(\text{Cr,W})\text{C}_6$  mixed carbide has formed. Fe-Exp2 powder,

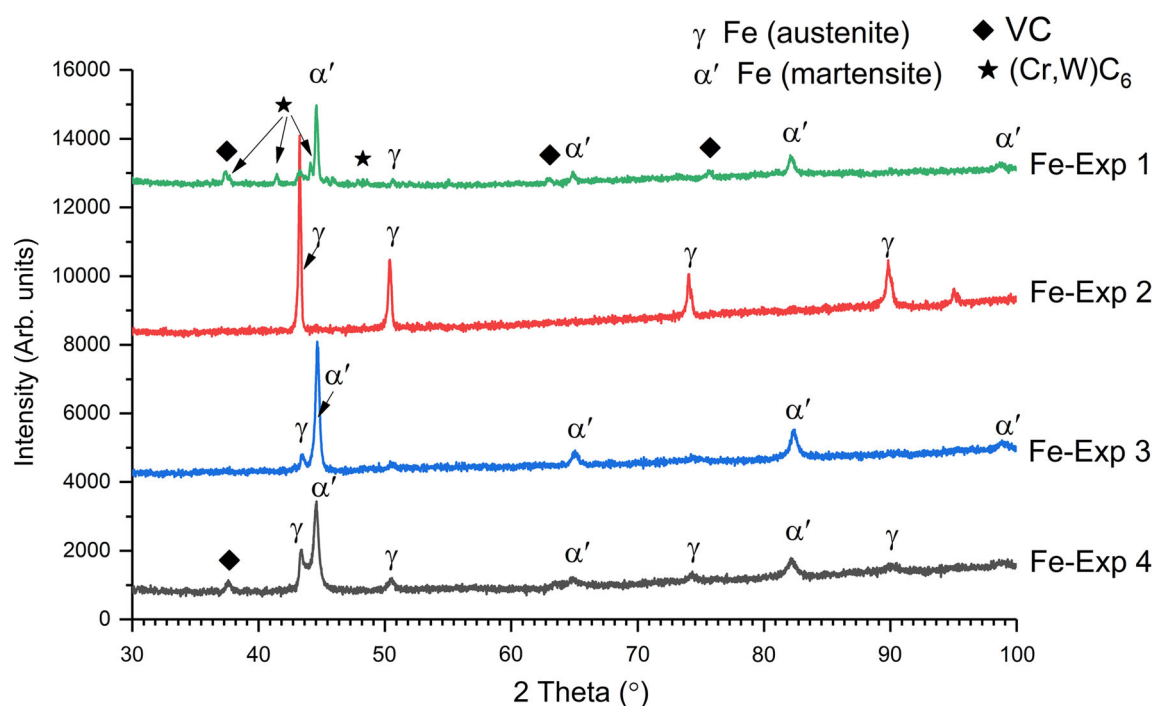


**Fig. 1** XRD analysis of the powders

on the other hand, contained only austenite peaks. The austenitic structure and the absence of carbide peaks suggest that the carbon and carbide-forming alloying elements were supersaturated in austenite as a solid solution instead of forming carbides. The carbon dissolved in austenite effectively lowers the formation temperature of martensite, which in this case seemed to be below room temperature; thus, martensite was not formed. Vanadium is a relatively strong carbide former, and it can form already in the melt during atomisation (Ref 27), resulting in grow of relatively large VC grains powders with high V content. The formation of carbide leads to a decrease in the carbon content in austenite, which increases the martensitic transformation temperature above room temperature, allowing the formation of a martensitic structure during quenching of atomised particle. Obviously, some retained austenite remains in the powders. As an example, the microstructure of Fe-Exp4 powders is presented in Fig. 2, where lumpy VC grains have formed in a martensitic matrix.

The backscatter SEM images of the coatings are shown in Fig. 3 and 4. The porosity of the coatings is presented in Table 3. WC-Com and CrC-Com coatings show a high content of either tungsten or chromium carbides. WC appears lighter in colour than the CoCr matrix, and  $\text{Cr}_3\text{C}_2$  appears darker than the NiCr matrix. WC coatings also show some micron size porosity. In WC coatings, there is only minor difference in carbide content between HVOF and HVAF. In contrast, for  $\text{Cr}_3\text{C}_2$  coatings, the carbide content of HVOF coatings is clearly higher than that of

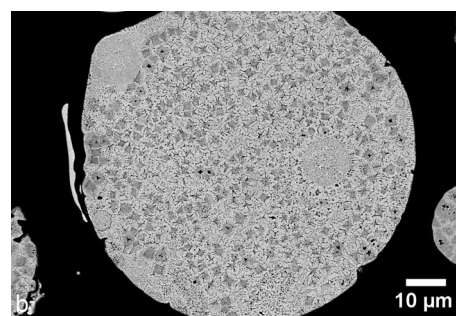
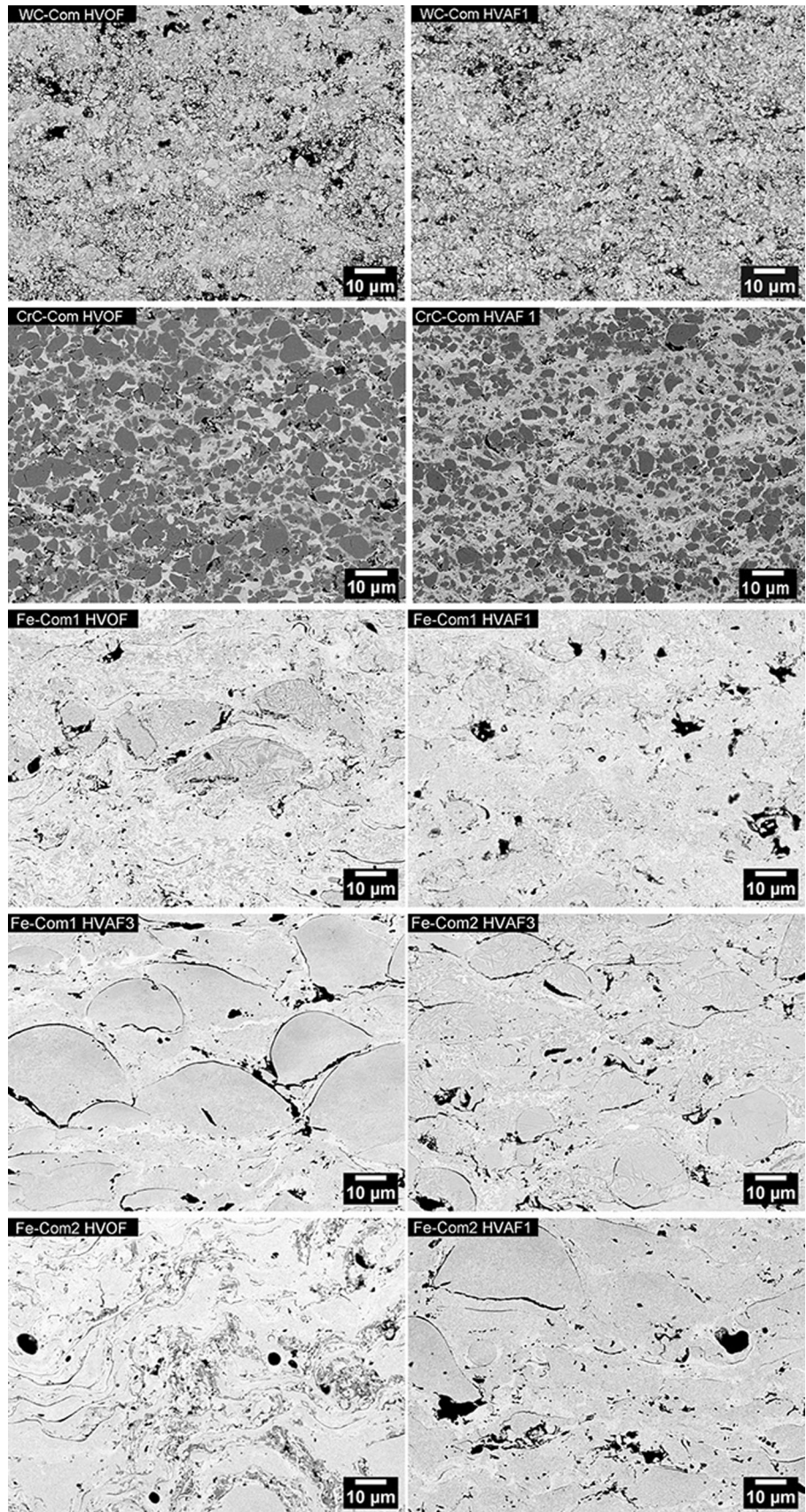


**Fig. 2** The cross-sectional backscatter image of the Nital 3% etched Fe Exp-4 powder particle, which reveals the lumpy VC-particles in the mainly martensitic Fe-matrix

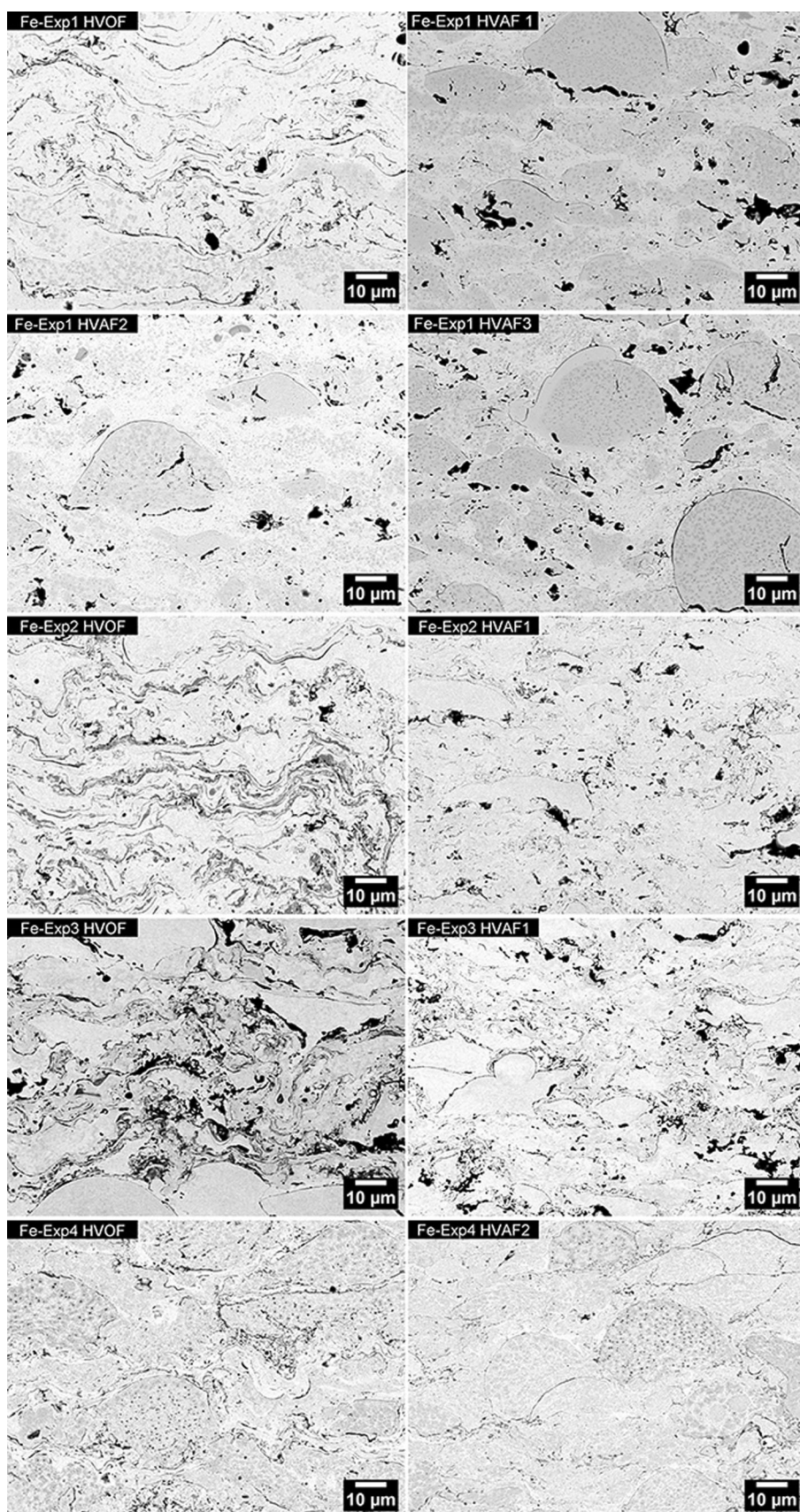
HVAF coatings. This is due to the fact that especially larger carbides tend to rebound and cause carbide loss when the matrix is not sufficiently molten to properly bind the carbide (Ref 30). In any case, the inherently high carbide contents of these agglomerated and sintered powders produce a coating with significantly more and larger carbides than visible in the microstructure of the atomized iron powders formed by melting. The hardness of the coatings is shown in Fig. 5. Coatings made from WC (WC-Com) and  $\text{Cr}_3\text{C}_2$  (CrC-Com) agglomerated and sintered powders were the hardest due to their high carbide content.

The hardness of iron-based coatings ranged between 530 and 830 HV and was influenced by both the proportion of hard phases and the spray equipment/spray parameters used. The carbides in atomized iron powders are formed in

**Fig. 3** Backscatter SEM images of the coatings made of commercial powders (Com)



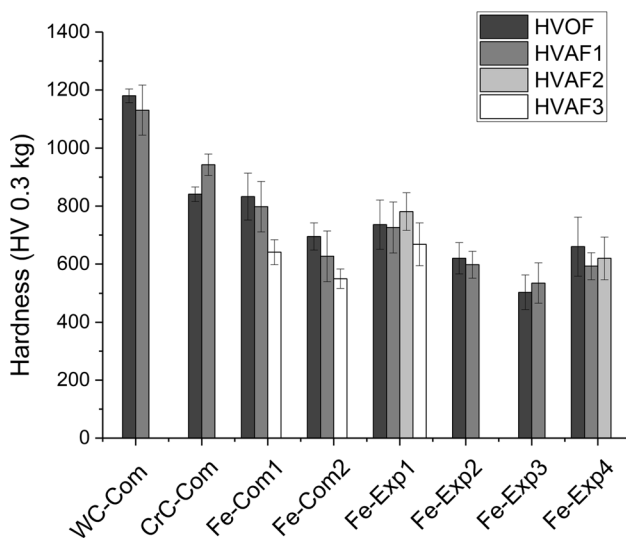
**Fig. 4** Backscatter SEM images of the coatings made of experimental powders (Exp)





**Table 3** Hardness, abrasion wear resistance, and cavitation erosion wear resistance of the coatings

Code	Hardness, HV, 0.3 kg	Cavitation erosion resistance, s mm <sup>-3</sup>	Abrasion wear resistance, s mm <sup>-3</sup>	Porosity, %
WC-Com HVOF	1180 ± 23	878	588	2.93
WC-Com HVAF1	1131 ± 86	16,799	1051	1.71
CrC-Com HVOF	841 ± 25	1349	240	2.07
CrC-Com HVAF1	943 ± 37	9360	849	0.73
Fe-Com1 HVOF	833 ± 81	7931	38	2.08
Fe-Com1 HVAF1	798 ± 87	8165	49	1.64
Fe-Com1 HVAF3	641 ± 43	5158	55	2.46
Fe-Com2 HVOF	695 ± 47	4814	28	1.17
Fe-Com2 HVAF1	627 ± 87	4643	36	3.48
Fe-Com2 HVAF3	550 ± 33	5941	32	4.17
Fe-Exp1 HVOF	736 ± 85	3254	52	1.50
Fe-Exp1 HVAF1	726 ± 88	4775	135	4.12
Fe-Exp1 HVAF2	781 ± 65	10,607	92	1.32
Fe-Exp1 HVAF3	668 ± 74	5844	146	4.72
Fe-Exp2 HVOF	620 ± 54	7398	20	1.89
Fe-Exp2 HVAF1	598 ± 46	11,371	19	0.99
Fe-Exp3 HVOF	503 ± 59	3751	26	4.30
Fe-Exp3 HVAF1	535 ± 69	12,056	23	3.10
Fe-Exp4 HVOF	660 ± 102	10,330	30	1.75
Fe-Exp4 HVAF1	620 ± 73	6271	30	3.99
Fe-Exp4 HVAF2	593 ± 46	5834	51	0.78

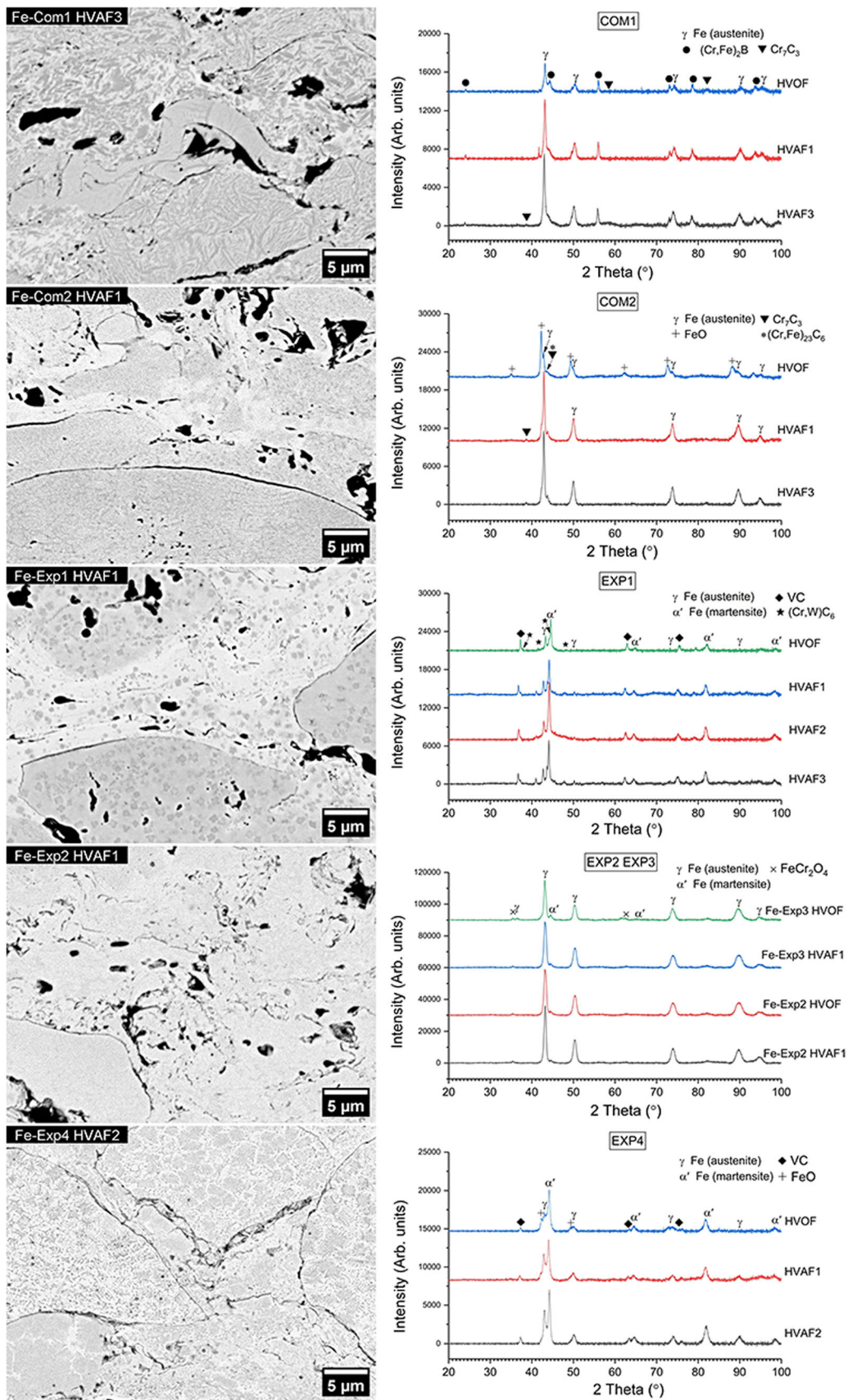
**Fig. 5** Hardnesses of coatings

the melt. In atomization, the cooling rate is relatively fast, so the carbides may not have time to form according to equilibrium and have no time to grow. Consequently, the carbon may remain supersaturated, or the carbides may remain fine. As a result, the carbide content and size of atomized powders are generally lower than those of

agglomerated powders, which clearly affects their hardness.

Coatings from Com 1 atomised Fe-powder, Fe-Com1 HVOF and Fe-Com1 HVAF, have a similar appearance. They show very small-sized carbides/borides in the lighter austenitic matrix in Fig. 3 and 6. According to XRD, in Fig. 6, the hard phases can be identified mainly as  $(Cr,Fe)_2B$  with very small amount of  $Cr_7C_3$ . The structure of the coating corresponds to the analyses of Milanti et al. in (Ref 14). Relatively large pores of about 2-10 mm are also seen in Fe-Com1 HVOF and Fe-Com HVAF1 coatings. The high flow rate parameters used for the 5L4 barrel for Com1 HVAF3 coating, appeared to produce high levels of unmelted particles in the coating. The unmelted particles in the coating had poor adhesion to surroundings, as shown in Fig. 3 by the high interlamellar porosity around unmelted particles. The reduced hardness of the Fe-Com1 HVAF3 coating is shown in Fig. 5.

Fe-Com2 coatings also have an austenitic Fe matrix alloyed with Cr, Ni and Mo. Both, Fe-Com2 HVAF1 and HVAF3, coatings have clear primary  $M_7C_3$  chromium carbide peaks in XRD-curves. However, in the hotter HVOF process Fe-Com2 HVOF the peaks around  $M_7C_3$  peaks in coatings are wider, which suggests that carbon and chromium from the carbides have partly dissolved in an



◀ **Fig. 6** XRD analysis of the coatings of iron-based alloys

austenite during the HVOF spraying leaving finely structured supersaturated austenitic solid solution in the coating, as shown by Sadeghimeresht et al. (Ref 31), or that the secondary carbide  $(\text{Fe,Cr})_6\text{C}_{23}$ , whose peaks are very close to theta angle of  $\text{Cr}_7\text{C}_3$  peak, has formed. The microstructure of the Fe-Com2 HVOF coating in Fig. 3 also has oxide clusters which, based on XRD, are chromium oxide. Oxides seemed to have a hardness enhancing effect in this case (Fig. 5).

The Fe-Exp1 alloy was designed to form multiple carbides on an austenitic-martensitic matrix. XRD-analysis (Fig. 6) shows the matrix to be predominantly martensite with some retained austenite. The alloying of Fe-Exp1 favours the formation of martensite because, unlike Fe-Com1 and Fe-Com2, it does not contain Ni, which is a strong austenite stabiliser, and it has formed stable VC already during atomisation, which reduced the amount of carbon in the austenite, thus lowering martensite start temperature as being presented earlier. The main carbide, VC, is clearly visible in microstructure and XRD in Fig. 6. The secondary carbide is  $(\text{Cr,W})\text{C}_6$  mixed carbide. With respect to spray parameters, HVOF 2 parameters with 4L4 nozzle gave highest hardness for Fe-Exp1 powder.

Exp-2 and Exp-3 have a similar composition to Böhler K110 tool steel. This alloy is hardenable in air, which in equilibrium would form a martensitic matrix with finely dispersed chromium and vanadium carbides (Ref 32). However, the atomized powder was predominantly austenitic due to rapid cooling during atomization. The composition of Exp-3 is the same as Exp-2, but it has been heat treated at 550 °C for 2 h to form martensite. XRD analysis of the coatings (Fig. 6) shows that the heat treatment of the powder did not result in a significant change in the microstructure of the coating, as no martensitic structure remained in the coatings made from martensitic Fe-Exp3 powder. The crystalline structures of coatings in Fig. 6 sprayed from Exp2 and Exp3 powders are identically almost entirely retained austenite when sprayed by both methods (HVOF and HVAF), regardless of whether the powder is austenite or martensite. This suggests that heat treatment of the powder at 550 °C forms carbides, which reduce the carbon content of the matrix and allow it to harden at room temperature, have mainly dissolved back into the matrix during the spraying process. This can be further confirmed by the fact that no carbides are visible in the coatings at SEM resolution, nor do the chromium carbide peaks show up in the coating XRD (Fig. 6). The retained austenite in the structure is possible because the carbon is not bound to the carbides, so the carbon content

of the austenite matrix remains high, lowering the martensite start temperature. Thus, in the coating carbon and other alloying elements are supersaturated in the solid solution, and retained austenite was formed instead of martensite. The distorted, supersaturated austenite in solid solution has a higher hardness than normal austenite because of high dislocation density and fine grain size of the solid solution.

It can be observed that there is a very clear difference between Exp2HVOF and Exp3HVOF coatings. In addition to the high proportion of unmelted particles, the porosity also seems to have increased significantly as a result of the heat treatment. It is known that the unmelted particle increases the porosity around it, as it causes so-called insufficient filling (Ref 33-36). The increase in the number of unmelted particles and thus the increase in porosity is presumably due to microstructural changes during heat treatment. As noted earlier, when discussing the heat treatment of powders, Fe-Exp3 powder has more carbide-bound carbon than Fe-Exp2 powder. According to the Fe-C equilibrium diagram, the solidus temperature of Fe-C alloy increases when the carbon content of iron falls below 2.14%. Consequently, melting of the iron matrix of the heat-treated powder is more difficult, and some of the larger particles may remain only partially melted in the spraying process. These partially melted particles may remain in the coating as round, slightly deformed particles. In addition to being difficult to melt, they also harden significantly as a result of heat treatment, making them difficult to deform. These factors seem to increase the porosity of Fe-Exp3 compared to Fe-Exp2. In Exp4, the matrix appears to contain varying amounts of visible VC in different splats. Carbides are more clearly visible in larger splats (originated from the atomised powder particles) than in smaller splats. In general, it appears that VC is relatively stable in spraying and that VC already present in the powders is well retained in the coating. Thus, it appears that the size of the VCs corresponds to the size that they form in powder particles of different sizes during atomization. Furthermore, the hardness of Exp4 coatings is lower compared to the hardness of Fe-Exp1 coatings, which probably emphasizes the role of secondary carbide formers which are present in Fe-Exp1.

In coatings (Fe-Com2 and Fe-Exp1-4), there is a clear difference between HVOF and HVAF. In HVOF coatings, well flattened splats with lamellar oxide bands around them are observed. Clusters of finer oxides can also be observed, and pull-outs in these oxide clusters. Also, in coatings made by the HVOF process, it is seen that the concentration differences are not visible in the most flattened splats, suggesting that the carbides have begun to dissolve. HVAF coatings have fewer flat splats and relatively many unmelted particles. For HVAF the porosity appears to be

due to poor filling in the vicinity of the unmelted particles, which seems to increase the porosity in some of the HVAF coatings, especially in Fe-Com2 HVAF1, Fe-Com2 HVAF3, Fe-Exp1 HVAF1, Fe-Exp1 HVAF3, and Fe-Exp4 HVAF1. It should be noted that the size distributions of Fe-Com2 powder and Fe-Exp4 powder were the same for HVOF and HVAF, which may explain the high number of unmelted particles in these coatings. It also highlights the importance of using correct size distribution for each process. Concerning HVAF coatings of Com2 and Exp4 powders it is likely that particle size distribution-spraying parameter combination did not result in the best achievable coating quality. Milanti et al. (Ref 19, 37) suggested that in HVAF processes the powder structure is relatively well preserved because the powder particles do not heat up as much, which could be confirmed in this study as well. On the other hand, the lower temperature of the HVAF process (and too coarse particle size distribution) seems to introduce some structural porosity in the coating. The difficulty of producing non-porous coatings from high strength Fe alloys with HVAF processes has also been shown before (Ref 31). In terms of porosity, a fine and narrow size distribution of such a powder, preferably 10-30  $\mu\text{m}$ , would seem to be advantageous for HVAF as the use of a coarser powder could result in unmelted particles remaining in the coating, around which porosity would increase due to insufficient filling. However, in case of 10-30  $\mu\text{m}$  fine iron powders, M3 should use a small combustion chamber to avoid powder clogging in the chamber. In addition, it was necessary to use a ceramic primary nozzle to prevent the powder from clogging the nozzle. In addition, M3 offers many different hardware configurations to influence the microstructure and properties of the coating. In this study, the optimal powder size-equipment configuration-injection parameter combination was not necessarily achieved for all coatings, especially if 15-45  $\mu\text{m}$  size fractions were used for HVAF.

### Wear Performance of Coatings

The hardness and wear resistances of coatings are presented in Table 3. Abrasion resistance versus hardness and cavitation erosion resistance versus hardness maps of the coatings are shown in Fig. 7(a) and (b). With respect to abrasive wear, coatings made of agglomerated chromium carbide and tungsten carbide powders are in a class of their own. The high carbide content of these coatings and the resulting hardness is responsible for their good abrasion resistance. This is further influenced by the relatively large size of the carbides in relation to the abrasive grain. For iron-based coatings from atomised powders the

simultaneous removal of the fine carbides and soft binder by cutting, contributes to the wear of these alloys (Ref 12). There is no significant difference in abrasion resistance between the iron coatings, although the hardness of the coatings varied between 500 and 800 HV. However, it is notable, that the abrasion resistance of Exp1 HVAF coatings is clearly better than that of other iron-based coatings. This can be explained by the microstructure of the coating, with relatively large vanadium carbides in a mixed austenitic-martensitic matrix, further reinforced with smaller tungsten-based carbides.

The cavitation erosion resistance of thermally sprayed coatings, as also observed in this study, is not so clearly dependent on hardness, since cavitation erosion is caused by a crack growth mechanism, which occurs mainly at the boundaries of weak lamellae and which, if continued, leads to the detachment of larger fracture zones (Ref 16). In contrast, the cavitation erosion resistance of thermally sprayed coatings has been found to be significantly affected by interlamellar cohesion and residual stresses (Ref 16, 17).

In the present study, it was noted that there were large differences in the cavitation resistance of the same coating material depending on the spraying method and the parameters used. It was also noted that the cavitation erosion resistance of the coatings varied significantly depending on the HVAF spray configurations used. These observations highlight the importance of optimising the spraying conditions. Based on this study, two clear process-related factors were identified that reduced the cavitation resistance of coatings. First, in HVOF spraying, iron oxide clusters (and possibly also lamellar boundary particles) adversely affect the cavitation erosion resistance of the coatings. Oxide clusters were particularly observed in Fe-Com2 HVOF and Fe-Exp4 HVOF coatings. Secondly, in the case of HVAF, the unmelted particles remaining in the structure proved to be detrimental to cavitation resistance, both by increasing interlamellar porosity and, presumably, by impairing interlamellar adhesion. Unmelted particles were particularly a problem in coatings with a coarse powder particle size distribution, such as in Fe-Com2 and Fe-Exp 4 HVAF coatings. For the same reason, it was found that the high flow parameters used in the 5L4 nozzle, HVAF 3, did not improve cavitation resistance.

In contrast, good cavitation erosion results (Fig. 7b) were obtained with the relatively soft iron-based HVAF coatings Fe-Exp2 HVAF and Fe-Exp3 HVAF. These coatings did not suffer from oxidation and were in the austenitic phase, which makes them strain hardenable. The cavitation resistance of these relatively soft iron-based coatings was significantly better than the very hard WC-

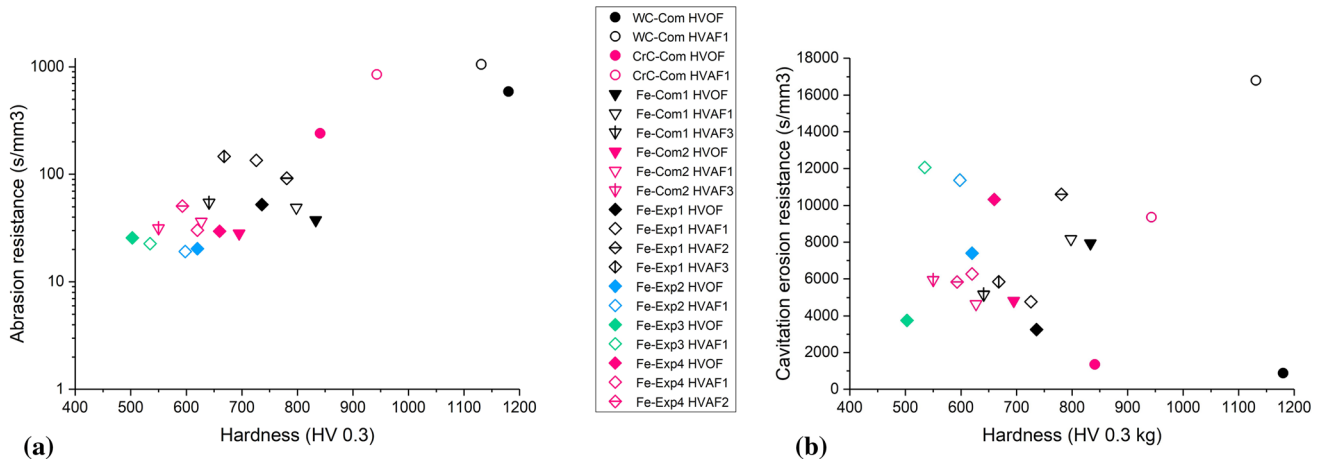


**Fig. 7** (a) Abrasion wear resistance—hardness plots of coatings, where Abrasion resistance in logarithmic scale and (b) cavitation erosion resistance—hardness plot of coatings (linear scale). Round

symbols represent the commercial carbide coatings, triangles commercial Fe-based coatings and quadrants experimental Fe-coatings

CoCr and Cr<sub>3</sub>C<sub>2</sub> coatings sprayed by HVOF, which may indicate that the phase transformations possibly prevents cavitation-induced crack growth and lower cavitation erosion.

The role of residual stress on cavitation resistance was not really investigated in this study, but it was found that there was a significant difference between HVAF sprayed and HVOF sprayed WC-CoCr coatings and Cr<sub>3</sub>C<sub>2</sub>-NiCr coatings. The cavitation resistance of HVAF coatings Fe-Exp1, Fe-Exp2 and Fe-Exp3 was also better than HVOF coatings. Previous studies have shown that HVAF spraying can induce significant compressive stresses in WC-CoCr coatings, which inhibit the cavitation crack growth and improves the cavitation resistance (Ref 17). High compressive stresses are result of the peening effect, which is associated with poor deposition efficiency, that was here observed with Cr<sub>3</sub>C<sub>2</sub> and WC HVAF coatings (thickness per amount of powder used). With Cr<sub>3</sub>C<sub>2</sub> HVAF coatings, also significant carbide loss was evident, which proves the compressive state in the coating. The compressive stress state formed on WC and CrC based coatings by the HVAF method, may partly explain their good cavitation resistance compared to the corresponding HVOF coatings. On the other hand, with respect to iron coatings, this study found that the thickness/pass of HVOF and HVAF coatings was at similar levels and the coating deposition rate was at an overall good level, and therefore, significant residual stress differences are not expected for them. In summary, this study shows that iron-based HVOF and HVAF coatings are an excellent option for applications requiring cavitation resistance, provided that sufficient attention is paid to the choice of alloy composition and spraying parameters.

### Conclusions

The abrasive wear and cavitation erosion resistance of HVOF and HVAF sprayed iron-based coatings that formed different precipitates in the austenitic and/or martensitic matrix was studied. The study concluded that:

- The abrasion resistance of Fe coatings was found to be significantly worse than WC-CoCr and Cr<sub>3</sub>C<sub>2</sub>-NiCr coatings, which was due to the comparatively lower carbide/hard phase proportion and small hard phase size of iron coatings.
- The cavitation resistance of Fe coatings was at a good level being better than that of HVOF sprayed WC-CoCr and Cr<sub>2</sub>C<sub>2</sub>-NiCr coatings. However, the cavitation resistance of the HVAF sprayed WC-CoCr coating was still better than that of the iron-based coatings.
- The different thermal history of the HVAF and HVOF processes produced different microstructures in the Fe coatings and thus affected the cavitation resistance. HVAF coatings produced better cavitation resistance in almost all cases and especially when the powder size distribution was below about 35 microns. This was assumed to be due to less oxidation of the HVAF coatings and thus better lamellar cohesion. Additively, the gun hardware configuration and its relation to the particle thermal history significantly contributed to good cavitation resistance.
- Oxide clusters, which were observed in some HVOF coatings, and unmelted particles, which were typically observed in HVAF coatings, appeared to be detrimental to the cavitation resistance of the coatings.

**Acknowledgment** The research was funded partly by Academy of Finland project “Enabling phenomena behind multihierarchical

strengthening of high kinetic sprayed metallic coatings” (HIER-ARCH, Decision NUM: 318064) and partly by Academy of Finland project “Materials Performance Competence Spearhead” (PerForMat, Decision NUM: 337941). Authors would like to thank Anssi Metsähonkala and Jarkko Lehti from Tampere University, Thermal Spray Center Finland (TSCF), Tampere, Finland, for spraying the coatings and Luka Valmu from Tampere University for carrying out the wear tests.

**Open Access** This article is licensed under a Creative Commons Attribution 4.0 International License, which permits use, sharing, adaptation, distribution and reproduction in any medium or format, as long as you give appropriate credit to the original author(s) and the source, provide a link to the Creative Commons licence, and indicate if changes were made. The images or other third party material in this article are included in the article’s Creative Commons licence, unless indicated otherwise in a credit line to the material. If material is not included in the article’s Creative Commons licence and your intended use is not permitted by statutory regulation or exceeds the permitted use, you will need to obtain permission directly from the copyright holder. To view a copy of this licence, visit <http://creativecommons.org/licenses/by/4.0/>.

## References

1. S. Uozato, K. Nakata, and M. Ushio, Evaluation of Ferrous Powder Thermal Spray Coatings on Diesel Engine Cylinder Bores, *Surf. Coat. Technol.*, 2005, **200**(7), p 2580-2586.
2. M. Hahn and A. Fischer, Investigation of Surface Fatigue of Thermally Sprayed Micro- and Nanocrystalline Cylinder Wall Coatings by Means of Cavitation Testing, *Int. J. Mater. Res.*, 2008, **99**(10), p 1079-1089.
3. M. Oksa, T. Varis, and K. Ruusuvoori, Performance Testing of Iron Based Thermally Sprayed HVOF Coatings in a Biomass-Fired Fluidised Bed Boiler, *Surf. Coat. Technol.*, 2014, **251**, p 191-200. <https://doi.org/10.1016/j.surfcoat.2014.04.025>
4. T. Varis, D. Bankiewicz, P. Yrjas, M. Oksa, T. Suhonen, S. Tuurna, K. Ruusuvoori, and S. Holmström, High Temperature Corrosion of Thermally Sprayed NiCr and FeCr Coatings Covered with a KCl-K<sub>2</sub>SO<sub>4</sub> Salt Mixture, *Surf. Coat. Technol.*, 2015, **265**, p 235-243.
5. M. Oksa, S. Tuurna, and T. Varis, Increased Lifetime for Biomass and Waste to Energy Power Plant Boilers with HVOF Coatings: High Temperature Corrosion Testing Under Chlorine-Containing Molten Salt, *J. Therm. Spray Technol.*, 2013, **22**(June), p 783-796.
6. G. Bolelli, B. Bonferroni, J. Laurila, L. Lusvarghi, A. Milanti, K. Niemi, and P. Vuoristo, Micromechanical Properties and Sliding Wear Behaviour of HVOF-Sprayed Fe-Based Alloy Coatings, *Wear*, 2012, **276-277**, p 29-47. <https://doi.org/10.1016/j.wear.2011.12.001>
7. G. Bolelli, T. Börner, A. Milanti, L. Lusvarghi, J. Laurila, H. Koivuluoto, K. Niemi, and P. Vuoristo, Tribological Behavior of HVOF- and HVOF-Sprayed Composite Coatings Based on Fe-Alloy + WC-12% Co, *Surf. Coat. Technol.*, 2014, **248**, p 104-112. <https://doi.org/10.1016/j.surfcoat.2014.03.037>
8. S. Dizdar and M. Kumar, Fe-Based Powder Alloys Deposited by HVOF and HVAF for Sliding Wear Applications, in Proceedings of International Thermal Spray Conference ITSC 2015, vol 2 (p 706-711, 2016).
9. S. Mahade, O. Aranke, S. Björklund, S. Dizdar, S. Awe, R. Mušálek, F. Lukáč, and S. Joshi, Influence of Processing Conditions on the Microstructure and Sliding Wear of a Promising Fe-Based Coating Deposited by HVAF, *Surf. Coat. Technol.*, 2021, **409**, p 126953.
10. S. Mahade, S.A. Awe, S. Björklund, F. Lukáč, R. Mušálek, and S. Joshi, Sliding Wear Behavior of a Sustainable Fe-Based Coating and Its Damage Mechanisms, *Wear*, 2022, **500-501**(April), p 204375. <https://doi.org/10.1016/j.wear.2022.204375>
11. K.H.Z. Gahr, Wear by Hard Particles, *Tribol. Int.*, 1998, **31**(10), p 587-596.
12. A. Ghabchi, T. Varis, E. Turunen, T. Suhonen, X. Liu, and S.P. Hannula, Behavior of HVOF WC-10Co<sub>4</sub>Cr Coatings with Different Carbide Size in Fine and Coarse Particle Abrasion, *J. Therm. Spray Technol.*, 2010, **19**(1-2), p 368-377.
13. A. Ghabchi, S. Sampath, K. Holmberg, and T. Varis, Damage Mechanisms and Cracking Behavior of Thermal Sprayed WC-CoCr Coating Under Scratch Testing, *Wear*, 2014, **313**(1-2), p 97-105.
14. A. Milanti, H. Koivuluoto, P. Vuoristo, G. Bolelli, F. Bozza, and L. Lusvarghi, Microstructural Characteristics and Tribological Behavior of HVOF-Sprayed Novel Fe-Based Alloy Coatings, *Coatings*, 2014, **4**(1), p 98-120.
15. M.S. Lamana, A.G.M. Pukaszewicz, and S. Sampath, Influence of Cobalt Content and HVOF Deposition Process on the Cavitation Erosion Resistance of WC-Co Coatings, *Wear*, 2018, **398-399**, p 209-219. <https://doi.org/10.1016/j.wear.2017.12.009>
16. V. Matikainen, S. Rubio Peregrina, N. Ojala, H. Koivuluoto, J. Schubert, Houdková, and P. Vuoristo, Erosion Wear Performance of WC-10Co<sub>4</sub>Cr and Cr<sub>3</sub>C<sub>2</sub>-25NiCr Coatings Sprayed with High-Velocity Thermal Spray Processes, *Surf. Coat. Technol.*, 2019, **370**, p 196-212.
17. T. Varis, T. Suhonen, J. Laakso, M. Jokipii, and P. Vuoristo, Evaluation of Residual Stresses and Their Influence on Cavitation Erosion Resistance of High Kinetic HVOF and HVAF-Sprayed WC-CoCr Coatings, *J. Therm. Spray Technol.*, 2020, **29**(6), p 1365-1381. <https://doi.org/10.1007/s11666-020-01037-2>
18. G. Bolelli, A. Milanti, L. Lusvarghi, L. Trombi, H. Koivuluoto, and P. Vuoristo, Wear and Impact Behaviour of High Velocity Air-Fuel Sprayed Fe-Cr-Ni-B-C Alloy Coatings, *Tribol. Int.*, 2016, **95**, p 372-390.
19. A. Milanti, H. Koivuluoto, and P. Vuoristo, Influence of the Spray Gun Type on Microstructure and Properties of HVAF Sprayed Fe-Based Corrosion Resistant Coatings, *J. Therm. Spray Technol.*, 2015, **24**, p 1312-1322.
20. W. Yuping, L. Pinghua, C. Chenglin, W. Zehua, C. Ming, and H. Junhua, Cavitation Erosion Characteristics of a Fe-Cr-Si-B-Mn Coating Fabricated by High Velocity Oxy-Fuel (HVOF) Thermal Spray, *Mater. Lett.*, 2007, **61**(8-9), p 1867-1872.
21. Y. Wu, P. Lin, G. Xie, J. Hu, and M. Cao, Formation of Amorphous and Nanocrystalline Phases in High Velocity Oxy-Fuel Thermally Sprayed a Fe-Cr-Si-B-Mn Alloy, *Mater. Sci. Eng. A*, 2006, **430**(1-2), p 34-39.
22. Z. Zhou, L. Wang, D.Y. He, F.C. Wang, and Y.B. Liu, Microstructure and Wear Resistance of Fe-Based Amorphous Metallic Coatings Prepared by HVOF Thermal Spraying, *J. Therm. Spray Technol.*, 2010, **19**(6), p 1287-1293.
23. D.J. Branagan, W.D. Swank, D.C. Haggard, and J.R. Fincke, Wear-Resistant Amorphous and Nanocomposite Steel Coatings, *Metall. Mater. Trans. A Phys. Metall. Mater. Sci.*, 2001, **32**(10), p 2615-2621.
24. D.J. Branagan, M. Breitsameter, B.E. Meacham, and V. Belashchenko, High-Performance Nanoscale Composite Coatings for Boiler Applications, *J. Therm. Spray Technol.*, 2005, **14**(2), p 196-204.
25. S. Kumar, J. Kim, H. Kim, and C. Lee, Phase Dependence of Fe-Based Bulk Metallic Glasses on Properties of Thermal Spray Coatings, *J. Alloys Compd.*, 2009, **475**(1-2), p 10-13.

26. F. Huang, J.-j Kang, W. Yue, X.-b Liu, Z.-q Fu, L.-n Zhu, D.-s She, G.-z Ma, H.-d Wang, J. Liang, W. Weng, and C.-b Wang, Effect of Heat Treatment on Erosion–Corrosion of Fe-Based Amorphous Alloy Coating Under Slurry Impingement, *J. Alloys Compd.*, 2020, **820**, p 1-9.
27. X. Li, Y. Liu, and T. Zhou, Improvement in Microstructure and Wear-Resistance of High Chromium Cast Iron/Medium Carbon Steel Bimetal with High Vanadium, *Mater. Res. Express*, 2021, **8**(4), p 46512. <https://doi.org/10.1088/2053-1591/abd968>
28. B. Wielage, H. Pokhmurska, T. Grund, S. Ahrens, A. Wank, G. Reisel, T.M. Schnick, and E. Deppe, Vanadium-Rich Iron-Based Thermal Spray Coatings for Combined Wear and Corrosion Protection, in Thermal Spray 2006 Proceeding of the International Thermal Spray Conference, vol. 83669 (p 1107-1112).
29. P. Vuoristo, Thermal spray coating processes, *Comprehensive Materials Processing*. M.S.J. Hashmi Ed., Elsevier Ltd, 2014, p 229-275
30. V. Matikainen, G. Bolelli, H. Koivuluoto, M. Honkanen, M. Vippola, L. Lusvarghi, and P. Vuoristo, A Study of Cr<sub>3</sub>C<sub>2</sub>-Based HVOF- and HVOF-Sprayed Coatings: Microstructure and Carbide Retention, *J. Therm. Spray Technol.*, 2017, **26**(6), p 1239-1256.
31. E. Sadeghimeresht, N. Markocsan, and P. Nylén, Microstructural Characteristics and Corrosion Behavior of HVOF- and HVOF-Sprayed Fe-Based Coatings, *Surf. Coat. Technol.*, 2017, **318**, p 365-373.
32. “Product Information of Boehler K110 Steel,” <https://www.boehler-edelstahl.com/en/products/k110/>, n.d.
33. L.M. Berger, Application of Hardmetals as Thermal Spray Coatings, *Int. J. Refract. Met. Hard Mater.*, 2015, **49**, p 360-354.
34. M. Oksa and J. Metsäjoki, Optimizing NiCr and FeCr HVOF Coating Structures for High Temperature Corrosion Protection Applications, *J. Therm. Spray Technol.*, 2015, **24**(3), p 436-453.
35. C.J. Li and G.J. Yang, Relationships Between Feedstock Structure, Particle Parameter, Coating Deposition, Microstructure and Properties for Thermally Sprayed Conventional and Nanostructured WC-Co, *Int. J. Refract. Met. Hard Mater.*, 2013, **39**, p 2-17.
36. T. Varis, T. Suhonen, M. Jokipii, and P. Vuoristo, Influence of Powder Properties on Residual Stresses Formed in High-Pressure Liquid Fuel HVOF Sprayed WC-CoCr Coatings, *Surf. Coat. Technol.*, 2020, **388**, p 125604.
37. A. Milanti, V. Matikainen, H. Koivuluoto, G. Bolelli, L. Lusvarghi, and P. Vuoristo, Effect of Spraying Parameters on the Microstructural and Corrosion Properties of HVOF-Sprayed Fe-Cr-Ni-B-C Coatings, *Surf. Coat. Technol.*, 2015, **277**, p 81-90. <https://doi.org/10.1016/j.surfcoat.2015.07.018>

**Publisher’s Note** Springer Nature remains neutral with regard to jurisdictional claims in published maps and institutional affiliations.